Phase diagrams of the classical Heisenberg fluid within the extended van der Waals approximation

A. Oukouiss and M. Baus
Faculté des Sciences, Case Postale 231, Université Libre de Bruxelles, B-1050 Bruxelles, Belgium
(Received 13 February 1997)

We use a simple van der Waals theory, suitably extended to the solid phase and to anisotropic interactions, to study the phase behavior of a system of particles with magnetic exchange interactions. A very rich phase behavior is found which indicates, in particular, that the ferromagnetic liquid phase is favored by increasing the range of both the magnetic exchange interactions and of the nonmagnetic interactions. This could well explain why it turns out to be difficult to find such a phase in simulations which use interactions which are cut off at finite range. [S1063-651X(97)05806-6]

PACS number(s): 64.70.−p, 05.70.Fh, 75.10.−b

I. INTRODUCTION

The relation between the Hamiltonian of a system and the form of the resulting phase diagram is the central theme of equilibrium statistical mechanics [1]. For systems with only pair interactions, to which we will restrict ourselves here, a small change in the range of the pair potential can already induce a qualitative change in the topology of the phase diagram [2]. This raises, therefore, the general question of how many topologically distinct phase diagrams can be generated from a given family of pair potentials. This question is of practical interest in situations where the pair potential can to some extent be prescribed (e.g., by chemical engineering techniques as is of current use in colloid science [3]) and a particular feature of the phase diagram is being sought for (e.g., the presence of a ferromagnetic fluid phase for the systems considered below). The determination of a complete phase diagram is, however, a very demanding task, and, therefore, the answer to the question raised is not generally available. In the particular case of systems of spherical molecules with simple pair interactions (of the Lennard-Jones type, say) convincing evidence has nevertheless been obtained recently that only three topologically distinct types of phase diagrams can be produced by such potentials. If the amplitude of the pair potential is used as temperature scale and the range of the repulsions is used to define the density scale, then the family of potentials considered did depend only on one additional parameter, fixing the range of the attractions (relative to the range of the repulsions). The results could then be classified into three categories corresponding to long-ranged, intermediate-ranged, and short-ranged attractions with phase diagrams exhibiting, respectively, a fluid-fluid critical point, no critical point, and an (isostructural) solid-solid critical point. The corresponding evidence is partly experimental [4], partly numerical [5], and partly theoretical [6]. Of particular interest here is the fact that the above scenario can also be faithfully reproduced by the van der Waals (vdW) theory when the latter is suitably extended to the solid phase [7].

In the present investigation we perform a similar study, but for somewhat more complex fluids composed again of spherical molecules but endowed now with internal degrees of freedom. When these internal states are of a discrete (quantum mechanical) nature such a system can and has been described in terms of an Ising model fluid [8] . Here we will instead represent the internal states by a continuous classical spin variable. The resulting model represents then a classical analog of the Heisenberg fluid [9]. Such a system can be thought of as a first approximation to more realistic systems with anisotropic interactions. The spin variable could then, for instance, point in the direction of some internal anisotropy such as a permanent electric or magnetic dipole moment. Phase diagrams of realistic dipolar systems, for example, are presently under intensive study but the difficulties specific to the dipole-dipole interactions [10] combined with the difficulties associated with obtaining phase diagrams leads to rather prohibitively elaborate calculations [11]. As far as is presently known, the Heisenberg fluid and the dipolar systems appear, however, to have many features in common [12]. Here we will therefore consider the Heisenberg fluid as a simple model for these more realistic systems. For concreteness, we will use the language of magnetism, and consider only ferromagnetic exchange interactions between the spins. In order to facilitate the computation of the many phase diagrams encountered, we will moreover describe this Heisenberg fluid within the vdW approximation, since the latter is known to lead to faithful results in the case without the magnetic interactions [7]. To this effect we will extend the vdW theory of [7] so as to allow for both translational and orientational degrees of freedom. The resulting theory is similar to that of [9], except for the treatment of the solid phases. In [9] the only distinction between the fluid and solid phases stems from the equation of state used to describe the hard-sphere repulsions, while the attractions are described by the same cohesion energy in both the fluid and solid phases. Here, as in [7], the attractions in the solid phase will be described instead in terms of their static lattice energy [13]. The main difference from [9] stems then from the fact that here the resulting vdW free energies do depend not only on the relative strengths of the interactions but also on the range of these interactions. As a consequence, the number of topologically distinct phase diagrams will be seen to be greatly enhanced.

In Sec. II we define the Heisenberg fluid in more detail. The extended vdW theory is summarized in Sec. III. The phase diagrams are discussed in Sec. IV while Sec. V contains our conclusions.

II. CLASSICAL HEISENBERG FLUID

We consider a system of identical molecules whose translational degrees of freedom can be described in terms of the position $\mathbf{r}$ of the center of mass of the molecule, while its orientational degrees of freedom will be described in terms of a classical spin variable $\mathbf{s}$, with $\mathbf{s}^2=1$. This spin variable can be viewed as defining the orientation of some internal property of the molecule, say its magnetic moment, and hence the vector $\mathbf{s}$ can point in any spatial direction. The interaction potential between two such molecules, $V(\mathbf{r}_1,\mathbf{r}_2;\mathbf{s}_1,\mathbf{s}_2)$, will be taken to be of the form

$$V(\mathbf{r}_1,\mathbf{r}_2;\mathbf{s}_1,\mathbf{s}_2)=V_0(r_{12})+V_m(r_{12};\mathbf{s}_1\cdot\mathbf{s}_2), \tag{1}$$

where $V_0(r_{12})$, with $r_{12}=|\mathbf{r}_1-\mathbf{r}_2|$, describes the isotropic (spin-independent) nonmagnetic interactions and $V_m(r_{12};\mathbf{s}_1\cdot\mathbf{s}_2)$ the anisotropic (spin-dependent) magnetic interactions. For the nonmagnetic interactions we take the usual vdW form [7]

$$V_0(r_{12})=\begin{cases}\infty, & x_{12}<1\\ -\epsilon_0\phi_0(x_{12}), & x_{12}\geqslant 1,\end{cases} \tag{2}$$

where $\phi_0(x_{12})\geqslant 0$, with $x_{12}=r_{12}/\sigma$ and $\phi_0(x_{12}=1)=1$, describes the attractions of amplitude $\epsilon_0>0$ between hard spheres of diameter σ. For the magnetic term of Eq. (1) we take exchange interactions [9]

$$V_m(r_{12};\mathbf{s}_1\cdot\mathbf{s}_2)=\mathbf{s}_1\cdot\mathbf{s}_2V_1(r_{12}), \tag{3}$$

where

$$V_1(r_{12})=\begin{cases}0, & x_{12}<1\\ -\epsilon_1\phi_1(x_{12}), & x_{12}\geqslant 1,\end{cases} \tag{4}$$

with $\phi_1(x_{12})\geqslant 0$, $\phi_1(x_{12}=1)=1$, as appropriate to ferromagnetic interactions of amplitude $\epsilon_1\geqslant 0$.

It is important to realize that potentials of form (1) contain no coupling between the translational $\{\mathbf{r}_1,\mathbf{r}_2\}$ and orientational $\{\mathbf{s}_1,\mathbf{s}_2\}$ variables. This coupling constitutes (together with its long range) the major difficulty of the dipole-dipole interactions (allowing, for instance, chain formation [14]). Potentials of form (1) do instead belong to the same family as the Maier-Saupe-McMillan potential, viz. $V_0(r_{12})+V_2(r_{12})P_2(\mathbf{s}_1\cdot\mathbf{s}_2)$, with $P_2(x)=\frac{1}{2}(3x^2-1)$, a Legendre polynomial, used to study the formation of liquid-crystalline phases induced by anisotropic attractions [15]. This mechanism is complementary to the formation of liquid-crystalline phases via anisotropic repulsions [16].

In what follows we will use Eqs. (1)–(4) with inverse-power functions for $\phi_l(x_{12})$ $(l=0,1)$. In particular, we will use $\phi_0(x)=1/x^n$, so that $n>3$ fixes the range of the isotropic attractions, and $\phi_1(x)=1/x^k$, so that $k>3$ fixes the range of the magnetic interactions. The final pair potential of our Heisenberg fluid can thus be written

$$V(\mathbf{r}_1,\mathbf{r}_2;\mathbf{s}_1,\mathbf{s}_2)=\epsilon_0\begin{cases}\infty, & x_{12}<1\\ -\{1/x_{12}^n+\mathbf{s}_1\cdot\mathbf{s}_2\,\gamma/x_{12}^k\}, & x_{12},\geqslant 1\end{cases} \tag{5}$$

where $x_{12}=r_{12}/\sigma$, while ϵ_0 fixes the energy scale and $\gamma=\epsilon_1/\epsilon_0$ measures the strength of the magnetic interactions. The reduced potential V/ϵ_0 thus depends on three positive parameters $\{\gamma,n,k\}$.

III. EXTENDED van der WAALS THEORY

As already stated above, computing phase diagrams is a very demanding task, certainly for anisotropic potentials such as Eq. (5). In view of this, here we will compute the free energy of the classical Heisenberg system defined by Eq. (5) within a mean-field van der Waals type of approximation which extends the considerations of [7] to anisotropic interactions. The resulting theory is very simple and flexible but nevertheless physically realistic when, as here, the major goal is to explore the influence of the potential parameters, such as $\{\gamma,n,k\}$ of Eq. (5), on the topology of the phase diagram.

A. Extension to anisotropic interactions

As is well known, the major steps of the vdW theory amount to using a free-volume approximation for the contribution of the hard-sphere repulsions, and a mean-field approximation for the contribution of the attractions [7]. The presence of anisotropic interactions of the general form $\Sigma_l V_l(r_{12})P_l(\mathbf{s}_1\cdot\mathbf{s}_2)$ yields a contribution to the average energy which, when treated in the same vdW mean-field approximation, reads

$$\tfrac{1}{2}\sum_l\int d\mathbf{r}_1\int d\mathbf{s}_1\int d\mathbf{r}_2\int d\mathbf{s}_2\rho_1(\mathbf{r}_1,\mathbf{s}_1)V_l(r_{12})\times P_l(\mathbf{s}_1.\mathbf{s}_2)\rho_1(\mathbf{r}_2,\mathbf{s}_2), \tag{6}$$

where $\rho_1(\mathbf{r},\mathbf{s})$ is the one-particle density. In view of the fact that these interactions do not couple the position and spin variables, we can likewise assume that $\rho_1(\mathbf{r},\mathbf{s})$ factorizes as

$$\rho_1(\mathbf{r},\mathbf{s})=\rho(\mathbf{r})h(\mathbf{s}), \tag{7}$$

where $\rho(\mathbf{r})$ is the center of mass density and $h(\mathbf{s})$ the angular distribution of the spin variable. For convenience, we take $\rho(\mathbf{r})$ to be normalized to the average density ρ in the volume V,

$$\int\frac{d\mathbf{r}}{V}\rho(\mathbf{r})=\rho, \tag{8}$$

and $h(\mathbf{s})$ normalized to 1:

$$\int d\mathbf{s}\,h(\mathbf{s})=1, \tag{9}$$

where

$$\int d\mathbf{s}\cdots\equiv\frac{1}{4\pi}\int_0^{2\pi}d\varphi\int_0^{\pi}d\theta\sin\theta\ldots, \tag{10}$$

with $\{\theta,\varphi\}$ being the polar angles of the unit vector $\mathbf{s}$ referred to a laboratory fixed coordinate system. Using Eq. (7), expression (6) factorizes as

$$\sum_l \left\{ \tfrac{1}{2} \int d\mathbf{r}_1 \int d\mathbf{r}_2 \rho(\mathbf{r}_1) V_l(r_{12}) \rho(\mathbf{r}_2) \right\} \times \left\{ \int d\mathbf{s}_1 \int d\mathbf{s}_2 h(\mathbf{s}_1) P_l(\mathbf{s}_1 \cdot \mathbf{s}_2) h(\mathbf{s}_2) \right\}, \quad (11)$$

where the radial factors can be treated as proposed in [7]. As to the angular factor of Eq. (11), we will assume the system to have uniaxial symmetry around the direction $\mathbf{n}$, with $\mathbf{n}^2=1$, of some infinitesimal external magnetic field so that

$$h(\mathbf{s}) \equiv h(\mathbf{s}\cdot\mathbf{n}) \equiv h(u), \quad (12)$$

where $\mathbf{s}\cdot\mathbf{n}=\cos\theta\equiv u$, since we can always put $\mathbf{n}$ in the direction of the polar z axis. The angular average $\langle\ \rangle$, of any axially symmetric function $g(u)$ of u then becomes

$$\langle g \rangle \equiv \int d\mathbf{s}\, h(\mathbf{s}) g(\mathbf{s}) = \int d\mathbf{s}\, h(u) g(u) = \tfrac{1}{2} \int_{-1}^{1} du\, h(u) g(u), \quad (13)$$

where we used Eqs. (10) and (12). The angular factor of Eq. (11) for $l=1$, as needed for Eq. (3), now becomes

$$\int d\mathbf{s}_1 \int d\mathbf{s}_2 h(\mathbf{s}_1) \mathbf{s}_1 \cdot \mathbf{s}_2 h(\mathbf{s}_2) = \langle \mathbf{s} \rangle^2 = \langle u \rangle^2, \quad (14)$$

since $\langle \mathbf{s} \rangle = \langle u \rangle \mathbf{n}$, as a result of the axial symmetry. Note that $\langle u \rangle$ is (proportional to) the average magnetization per particle.

B. Magnetic vdW free energy

For a system of N particles enclosed in a volume V at the equilibrium temperature T, the contribution of the angular degrees of freedom to the Helmholtz free energy, $F(N,V,T)$, will consist of the orientational entropy contribution

$$N k_B T \int d\mathbf{s}\, h(\mathbf{s}) \ln h(\mathbf{s}) \equiv N k_B T \langle \ln h(u) \rangle, \quad (15)$$

as induced by Eq. (7), k_B being Boltzmann's constant, and the mean-field exchange energy contribution of Eq. (3),

$$\langle u \rangle^2 \left\{ \tfrac{1}{2} \int d\mathbf{r}_1 \int d\mathbf{r}_2 \rho(\mathbf{r}_1) V_1(r_{12}) \rho(\mathbf{r}_2) \right\}, \quad (16)$$

as results of Eqs. (6) and (11). Introducing the reduced (Helmholtz) free energy per particle, $f=F/N\epsilon_0$, we have from Eqs. (15) and (16) for the magnetic contribution, say $\overline{f_m}$, to f,

$$\overline{f_m} = t \langle \ln h(u) \rangle - \gamma \phi_1 \langle u \rangle^2, \quad (17)$$

where $t=k_BT/\epsilon_0$ is the reduced temperature T, and ϵ_0 the amplitude defined in Eq. (2), $\gamma=\epsilon_1/\epsilon_0$, and

$$\phi_1 = \frac{1}{2N} \int d\mathbf{r}_1 \int d\mathbf{r}_2 \rho(\mathbf{r}_1) \phi_1(r_{12}/\sigma) \rho(\mathbf{r}_2), \quad (18)$$

where $\phi_1(x_{12})$ is the exchange integral of Eq. (4). In Eq. (18) we have, as explained in [7], $\rho(\mathbf{r}) \equiv \rho$ for a fluid phase and $\rho(\mathbf{r}) \equiv \Sigma_j \delta(\mathbf{r}-\mathbf{r}_j)$ for a crystalline solid of lattice sites $\{\mathbf{r}_j\}$. Equation (17) represents the magnetic free energy of a system with a prescribed angular distribution $h(u)$, hence a prescribed magnetization $\langle u \rangle$. In order to find the true equilibrium distribution, h_0, and the corresponding equilibrium magnetization $\langle u \rangle_0$, we now minimize Eq. (17) with respect to $h(u)$. The resulting extremum condition can be written

$$t[C + \ln h_0(u)] = 2\gamma\phi_1 u \langle u \rangle_0, \quad (19)$$

where the constant C is fixed by the normalization condition (9). The solution to Eq. (19) can be written in the standard mean-field form

$$h_0(u) = \frac{e^{qu}}{N(q)}, \quad (20)$$

where

$$N(q) = \tfrac{1}{2} \int_{-1}^{1} du\, e^{qu} = \frac{\sinh q}{q} \quad (21)$$

fixes the normalization $[C=\ln N(q)]$, and q is determined self-consistently by Eq. (19) or, equivalently,

$$tq = 2\gamma\phi_1 L(q), \quad (22)$$

where we used the identity

$$\langle u \rangle_0 = \frac{\partial \ln N(q)}{\partial q} \equiv L(q), \quad (23)$$

with

$$L(q) = \coth q - \frac{1}{q}, \quad (24)$$

the Langevin function. Switching from the order parameter q to the equilibrium magnetization per particle, $m=\langle u \rangle_0$, as our new order parameter we can rewrite the self-consistency condition (22) as

$$m = L\left(2\frac{\gamma}{t} \phi_1 m \right), \quad (25)$$

where we used $q=2(\gamma/t)\phi_1 m$, as follows from Eqs. (22) and (23). As can be seen from Fig. 1, Eq. (25) has a unique solution

$$m = 0 \quad \text{for} \quad 0 \leqslant 2\frac{\gamma}{t}\phi_1 \leqslant 3, \quad (26)$$

and also a nonzero solution

$$0 < m \leqslant 1 \quad \text{for} \quad 3 < 2\frac{\gamma}{t}\phi_1, \quad (27)$$

where the borderline

$$2\gamma\phi_1 = 3t, \quad (28)$$

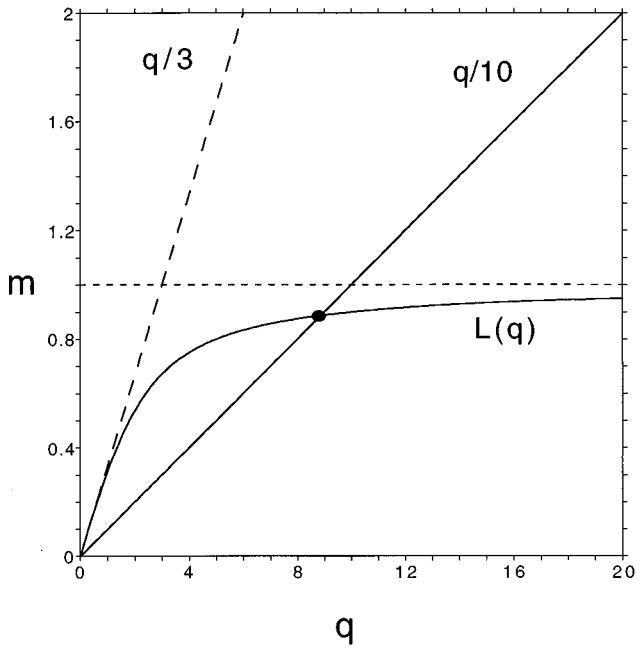

FIG. 1. Graphical representation of the solution of the self-consistency equation (25), $m=L(q)$ and $q=am$, indicating that a nonzero magnetization ($m\neq 0$) can exist only for $a>3$.

which separates the zero and nonzero magnetization solutions, defines the Curie line of the phase considered. Note that, whereas in [9] all phases have the same Curie line, here the fluid and solid phases have a different Curie line determined by ϕ_1 of Eq. (18). Note also that close to the Curie line the solution of Eq. (25) reads

$$m^2\cong\frac{5}{9}\left(2\frac{\gamma}{t}\phi_1-3\right),\quad 2\gamma\phi_1\gtrsim 3t, \tag{29}$$

whereas far away from the Curie line we have

$$m^2\cong 1-\frac{t}{\gamma\phi_1},\quad 2\gamma\phi_1\gg 3t, \tag{30}$$

where $\mp m$ does denote here the same ferromagnetic phase .

Finally, the magnetic contribution to the free energy of the equilibrium state, say f_m, can be obtained by evaluating f_m of Eq. (17) with Eq. (20). The result can be written

$$f_m=t\left\{\frac{q}{2}L(q)-\ln N(q)\right\}, \tag{31}$$

with q determined from Eq. (22) or, equivalently, $q=2(\gamma/t)\phi_1 m$, and m determined from Eq. (25).

C. Total vdW free energy

To obtain the total free energy of the Heisenberg system, $f=f_0+f_m$, we add the magnetic free energy, f_m of Eq. (31), to the vdW free energy, say f_0, corresponding to the nonmagnetic interaction $V_0(r_{12})$ of Eq. (1). The latter was discussed in detail in [7]. Within the vdW approximation we have

$$f_0=t[\ln(\rho\Lambda^3)-1]-t\ln\alpha(\rho)-\phi_0, \tag{32}$$

where the first term represents the ideal gas contribution from the translational degrees of freedom, Λ being the thermal de Broglie wavelength, $\rho=N/V$ the average density, and $t=k_BT/\epsilon_0$ the reduced temperature. The second term of Eq. (32) represents the free-volume entropy due to the hard-sphere (HS) repulsions of Eq. (2). In particular, we have (see [7])

$$\alpha(\rho)=(1-\rho/\rho_0) \tag{33}$$

for a fluid phase, with $(\pi/6)\rho_0\sigma^3=0.495$ being the packing fraction above which the fluid becomes unstable, and

$$\alpha(\rho)=\left[1-\left(\frac{\rho}{\rho_{cp}}\right)^{1/3}\right]^3 \tag{34}$$

for a solid phase, with $(\pi/6)\rho_{cp}\sigma^3=0.74$ the packing fraction above which a close-packed crystal becomes unstable. Finally, the last term of Eq. (32) represents the contribution of the nonmagnetic attractions:

$$\phi_0=\frac{1}{2N}\int d\mathbf{r}_1\int d\mathbf{r}_2\rho(\mathbf{r}_1)\phi_0(r_{12}/\sigma)\rho(\mathbf{r}_2), \tag{35}$$

with $\phi_0(x_{12})$ defined by Eq. (2). For a fluid phase, $\rho(\mathbf{r})\equiv\rho$, and Eq. (35) reduces to the cohesion energy

$$\phi_0=2\pi\rho\sigma^3\int_1^\infty dx\,x^2\phi_0(x), \tag{36}$$

while for a solid phase, $\rho(\mathbf{r})\equiv\Sigma_j\delta(\mathbf{r}-\mathbf{r}_j)$, and Eq. (35) reduces to the lattice energy

$$\phi_0=\tfrac{1}{2}\sum_j\ \phi_0(x_j), \tag{37}$$

where the sum runs overs the lattice sites, $r_j/\sigma=x_j>1$, of a periodic lattice without defects, r_j being the distance of site j to the site at the origin. Similar expressions hold for ϕ_1 of Eq. (18), but with $\phi_0(x)$ of Eq. (2) replaced by $\phi_1(x)$ of Eq. (4). For the inverse-power functions of Eq. (5) we have thus [see Eq. (36)]

$$\phi_0=\frac{2\pi\rho\sigma^3}{n-3},\quad \phi_1=\frac{2\pi\rho\sigma^3}{k-3} \tag{38}$$

for a fluid phase, and [see Eq. (37)]

$$\phi_0=\frac{\alpha_n}{2}\left(\frac{\rho}{\rho_{\rm cp}}\right)^{n/3},\quad \phi_1=\frac{\alpha_k}{2}\left(\frac{\rho}{\rho_{\rm cp}}\right)^{k/3} \tag{39}$$

for a crystal of close-packing density $\rho_{\rm cp}$ and Madelung constant α_m:

$$\alpha_m=\sum_j\left(\frac{x_1}{x_j}\right)^m,\quad m=n,k, \tag{40}$$

with $x_j\geqslant x_1$ and x_1 the reduced nearest neighbor distance ($\rho=\rho_{\rm cp}/x_1^3$).

IV. PHASE DIAGRAMS

Within the extended vdW theory of Sec. III, a system of molecules interacting via the pair potential (5) of the Heisenberg model is described by the following reduced Helmholtz free energy per particle, $f=F/N\epsilon_0$:

$$f=t[\ln(\rho\Lambda^3)-1]-t\ln\alpha(\rho)-\phi_0+t\left\{\frac{q}{2}L(q)-\ln N(q)\right\}, \tag{41}$$

with q determined by the self-consistency equations

$$q=2\frac{\gamma}{t}\phi_1 m, \quad m=L(q), \tag{42}$$

where we used the notation of Sec. III. For a system of number density ρ and reduced temperature $t=k_BT/\epsilon_0$, Eqs. (41) and (42) yield $f=f(\rho,t)$, and from f we obtain the pressure p and chemical potential μ using the well-known thermodynamic relations

$$p=\epsilon_0\rho^2\frac{\partial f}{\partial\rho}, \quad \mu=\epsilon_0 f+p/\rho, \tag{43}$$

where $\overline{\mu}=\mu/\epsilon_0$ and $p=\overline{p}\sigma^3/\epsilon_0$ are the corresponding dimensionless quantities. Below we will also use the packing fraction $\eta=(\pi/6)\rho\sigma^3$ as the reduced density variable. The two-phase equilibrium conditions can then be written

$$p_1(\rho_1,t)=p_2(\rho_2,t), \tag{44}$$

$$\mu_1(\rho_1,t)=\mu_2(\rho_2,t), \tag{45}$$

where the indexes 1 and 2 refer, respectively, to phases 1 and 2. Equations (44) and (45) are equivalent to the double tangent construction on the free energies obtained from Eqs. (41) and (42). When more then one transition is possible, the equilibrium transition is found by constructing the convex envelope to the free energies.

A. Paramagnetic and ferromagnetic fluid phases

We first consider the case where both phases 1 and 2 of Eqs. (44) and (45) are fluid phases. In this case the thermodynamics follows from Eqs. (41) and (42) by using Eq. (33) for $\alpha(\rho)$ and (38) for ϕ_0 and ϕ_1. Simple explicit expressions can again be obtained, such as

$$\frac{p}{\rho\epsilon_0}=\frac{t}{\alpha(\rho)}-\phi_0-m^2\gamma\phi_1 \tag{46}$$

for the pressure of the fluid phases. In Eq. (46) the equilibrium magnetization, $m=m(\rho,t)$, is obtained by solving Eq. (42), hence yielding $p=p(\rho,t)$, as needed for Eq. (44), and similarly for $\mu=\mu(\rho,t)$ by using Eq. (43). Here the Curie line $t=(2/3)\gamma\phi_1$ of Eq. (28) becomes a straight line in the ρ-t plane, $t=(4\pi/3)(\gamma\rho\sigma^3/k-3)$, or

$$t=\overline{\gamma}\eta, \quad \overline{\gamma}=\frac{8}{k-3}\gamma, \tag{47}$$

where η is the packing fraction. It then results from Eqs. (26) and (27) or Fig. 1 that for $t/\eta>\overline{\gamma}$ the fluid phases are paramagnetic ($m=0$), while for $t/\eta<\overline{\gamma}$ we have $m\neq 0$ and the fluid phases are hence ferromagnetic. On the Curie line, $t/\eta=\overline{\gamma}$, we have a paramagnetic-ferromagnetic transition which is continuous for $t>t_1$ and discontinuous for $t<t_1$ where $\{t=t_1,\eta=\eta_1\}$ denote a tricritical point (TCP) where the compressibility diverges ($\partial p/\partial\rho=0$). Using Eqs. (46) and (47), we obtain, for this TCP,

$$t_1=\overline{\gamma}\eta_1, \quad \eta_1=\left(1-\frac{1}{\left(\frac{5}{2}+\frac{3}{\gamma^*}\right)^{1/2}}\right)\eta_0, \tag{48}$$

where $\eta_0=(\pi/6)\rho_0\sigma^3\simeq 0.495$ as in Eq. (33), and $\gamma^*=\gamma\phi_1/\phi_0$ or

$$\gamma^*=\gamma\frac{n-3}{k-3}=\frac{n-3}{8}\overline{\gamma}, \tag{49}$$

where we used Eq. (38). The point of the Curie line (47) where the compressibility diverges is termed tricritical, although in zero external field the ferromagnetic phase is $\pm m$ degenerate. In the paramagnetic region ($m=0$), Eq. (46) also embodies the standard liquid-gas transition [7], with terminates in the vdW critical point (CP) with coordinates (t_c,η_c):

$$t_c=\frac{32}{3(n-3)}\eta_c, \quad \eta_c=\frac{\eta_0}{3}. \tag{50}$$

Combining this paramagnetic gas (pg)–paramagnetic liquid (pl) transition with the above paramagnetic fluid (pf)–ferromagnetic fluid (ff) transition, one finally obtains the phase diagram of the fluid phases in the entire η-t plane. Using Eqs. (44) and (45), it is easily seen that this phase diagram does not depend on the three parameters $\{\gamma,n,k\}$ separately but only on the combination $\gamma^*=\gamma(n-3)/(k-3)$. According to the value of γ^* there are three topologically distinct types of phase diagrams (see Fig. 2). For $0<\gamma^*<\gamma_1^*\simeq 0.55$ all the phase diagrams have a pg-pl transition at the higher temperatures, and a first-order pg-fl (ferromagnetic liquid) transition at the lower temperatures with the pg-pl transition ending in a CP and the first-order pg-fl transition ending in a critical end point where the Curie line describing the continuous pf-ff transition hits the first-order phase boundary. For $\gamma_1^*<\gamma^*<\gamma_3^*\simeq 0.85$ all the phase diagrams have a pg-fl transition for temperatures below that of a pg-pl-fl triple line. For temperatures above this triple point temperature there is both a pg-pl transition ending in a CP and a first-order pl-fl transition ending in a TCP. For $\gamma_1^*<\gamma^*<\gamma_2^*\simeq 0.727$ the TCP temperature is below the CP temperature, whereas the converse is true for $\gamma_2^*<\gamma^*<\gamma_3^*$. Finally, for $\gamma_3^*<\gamma^*$ all the phase diagrams contain only a first-order pg-fl transition ending in a TCP above which it becomes a continuous pf-ff transition along the Curie line. This scenario is identical to the one found by Hemmer and Imbro [9], except for the values of $\{\gamma_1^*,\gamma_3^*\}$. Indeed, for fluid phases the present theory is identical to that of Hemmer and Imbro, except for the fact that they did use

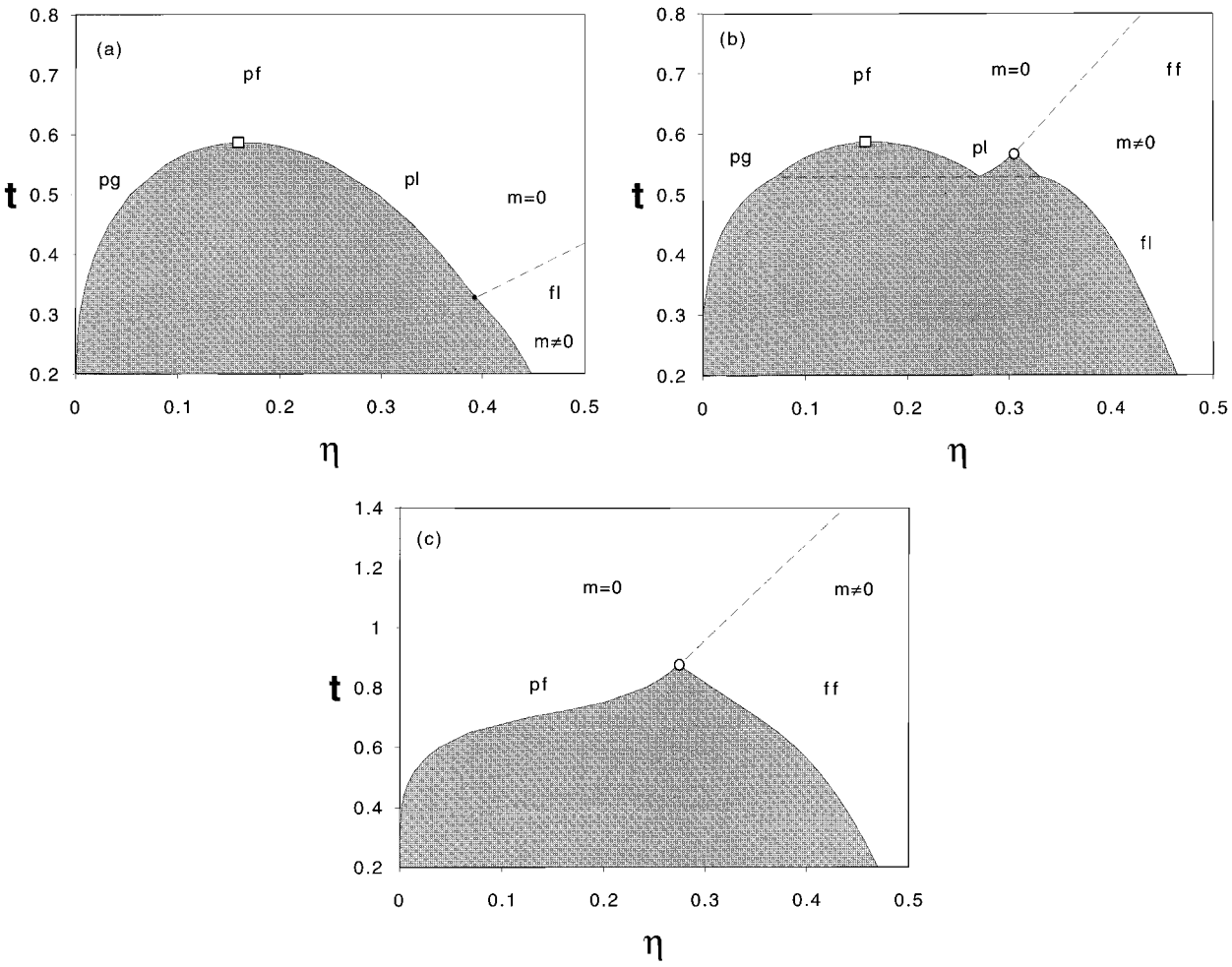

FIG. 2. The three topologically distinct types of phase diagrams in the reduced temperature ($t=k_BT/\epsilon_0$) reduced density [$\eta=(\pi/6)\sigma^3\rho$] plane as obtained from the free energy (41) when only fluid phases are considered. (a) A critical point (CP: open square) is seen to separate the low-temperature paramagnetic gas (pg) and paramagnetic liquid (pl) phases from the high-temperature paramagnetic fluid (pf) phases. The Curie line (dashed line) which separates the paramagnetic fluid (pf) from the ferromagnetic fluid (ff) phases ends in a critical end point (CEP: black dot), below which the pg-pl and pf-ff transitions are replaced by a pg-fl (ferromagnetic liquid) transition. (The diagram shown here corresponds to $\gamma^*=0.3$.) (b) The CEP of diagram (a) has been transformed into a tricritical point (TCP: open circle) where the pl-fl transition ceases to be first order and becomes continuous at higher temperatures. The TCP temperature is below the CP temperature for $\gamma^*\leqslant 0.73$, and above it for $\gamma^*>0.73$. There is thus more than one type of phase diagram in this category. In all cases there is also a pg-pl-fl triple line. (The diagram shown corresponds to $\gamma^*=0.7$.) (c) The pg-pl transition of (b) has become metastable, and only the pf-ff transition survives. (The case shown corresponds to $\gamma^*=1.2$.)

the Carnahan-Starling equation of state to describe the HS fluid instead of the simple free-volume expression (33) used here. This difference shifts the $\{\gamma_1^*,\gamma_3^*\}$ values from $\{0.55,0.85\}$, as found here, to $\{0.38,0.63\}$, as found by them. The Carnahan-Starling equation of state is clearly superior to the free-volume approximation (33) but the latter keeps the calculations simple enough to allow us to evaluate the coordinates of the TCP [see Eq. (48)] and CP [see Eq. (50)] explicitly, whereas the former does not. Finally, it is also worthwhile observing that the present scenario is qualitatively identical to the one predicted by Zhang and Widom [16] and Groh and Dietrich [11] for the fluid phases of dipolar systems.

B. Paramagnetic and ferromagnetic solid phases

From Sec. IV A it is seen that for $\gamma_3^*<\gamma^*$ the pf-ff transition preempts the pg-pl transition. In a similar manner the fluid(f)−solid(s) transition can still preempt this pf-ff transition. To answer the question whether a (stable) ferromagnetic fluid phase is present in the phase diagram, it is thus essential to include both fluid and solid phases. Before considering the complete phase diagram in Sec. IV C, we devote this section to the case where both phases in Eqs. (44) and (45) are solid phases. The thermodynamics is then still given by Eqs. (41) and (42), but now using Eq. (34) for $\alpha(\rho)$ and Eq. (39) for ϕ_0 and ϕ_1. The stable lattice structure is seen to be a compact lattice which we take to be of the face-centered-cubic (fcc) type. The resulting solid-solid transitions are then isostructural fcc-fcc transitions [7]. The corresponding equation of state of these solids can again be obtained in simple terms from Eq. (43), yielding

$$\frac{p}{\rho\epsilon_0}=\frac{t}{1-(\rho/\rho_{\rm cp})^{1/3}}-\frac{n}{6}\alpha_n(\rho/\rho_{\rm cp})^{n/3}-\frac{k}{6}\alpha_k(\rho/\rho_{\rm cp})^{k/3}m^2\gamma, \tag{51}$$

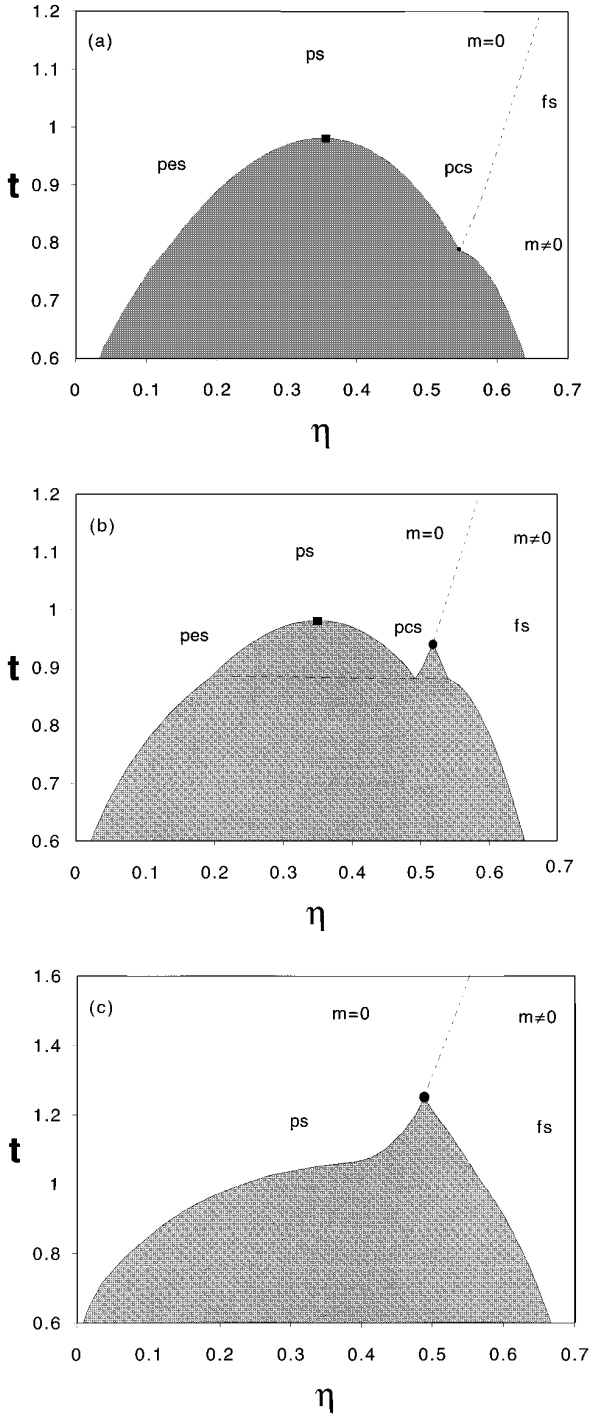

FIG. 3. The same as Fig. 2, but for the case where Eq. (41) is restricted to solid phases only. Here the *g-l* transition of Fig. 2 is replaced by an iso-structural transition between an expanded solid (es) and a condensed solid (cs) of the same compact crystal structure. The paramagnetic (expanded or condensed) solid phases (ps) are separated from the ferromagnetic solid (fs) phases by a new Curie line (dashed line). (a) A new CP (filled square) terminates the pes-pcs transition, while a new CEP (black dot) terminates the Curie line of the solids. (The case shown corresponds to $\gamma=0.3$ and $k=n=6$). (b) A new TCP (filled circle) terminates the first-order pcs-fs transition. There also is a pes-pcs-fs triple line. (The case shown corresponds to $\gamma=0.4$ and $k=n=6$). (c) Only the ps-fs transition survives. (The case shown corresponds to $\gamma=0.6$ and $k=n=6$).

where α_r is the Madelung constant of the fcc lattice for an inverse power potential of index $r=(n,k)$. As can be seen from Eq. (40), α_r tends to 12, the number of nearest neighbors of the fcc lattice, for large r values. Here the Curie line (28) becomes

$$t=\hat{\gamma}\eta^{k/3}, \quad \hat{\gamma}=\tfrac{1}{3}\alpha_k\gamma/\eta_{\rm cp}^{k/3} \tag{52}$$

with $\eta_{\rm cp}\equiv(\pi/6)\rho_{\rm cp}\sigma^3=\pi/3\sqrt{2}$ for a compact lattice. For $t/\eta^{k/3}>\hat{\gamma}$, the solid phases are paramagnetic ($m=0$), while for $t/\eta^{k/3}<\hat{\gamma}$, they are ferromagnetic ($m\neq 0$). On the Curie line, $t=\hat{\gamma}\eta^{k/3}$, the paramagnetic solid (ps) ferromagnetic solid (fs) transition becomes continuous above a new TCP of coordinates (t_2,η_2), given by Eq. (51) as

$$t_2=\hat{\gamma}\eta_2^{k/3}, \quad \eta_2=x^3\eta_{\rm cp} \tag{53}$$

with x a solution of

$$\frac{\left(1-\frac{2}{3}x\right)}{(1-x)^2}=\frac{5}{2}\left(\frac{k}{3}\right)^2+\frac{n\left(1+\frac{n}{3}\right)\alpha_n}{2\gamma\alpha_k}x^{n-k}. \tag{54}$$

When $n=k$, Eq. (54) yields

$$x=\left(\frac{3K-1}{3K}\right)-\left\{\left(\frac{3K-1}{3K}\right)^2-\left(\frac{K-1}{K}\right)\right\}^{1/2}, \tag{55}$$

with

$$K=\frac{5}{2}\left(\frac{k}{3}\right)^2+\frac{k}{2\gamma}\left(1+\frac{k}{3}\right). \tag{56}$$

In the region of the paramagnetic solids ($m=0$) there is an isostructural transition between a paramagnetic expanded solid (pes) and a paramagnetic condensed solid (pcs) which terminates in a new CP of coordinates (t_c',η_c'):

$$t_c'=n\left(1+\frac{n}{3}\right)\alpha_n y^n\frac{(1-y)^2}{\left(1-\frac{2}{3}y\right)}, \quad \eta_c'=y^3\eta_{\rm cp}, \tag{57}$$

with y given by

$$y\equiv\left(\frac{5n+4}{4(n-1)}\right)-\left\{\left(\frac{5n+4}{4(n-1)}\right)^2-\left(\frac{3n}{2(n-1)}\right)\right\}^{1/2}. \tag{58}$$

Whereas the overall behavior of the solid-solid phase diagrams is similar to that of the fluid-fluid phase diagrams, (t_c,η_c) and (t_1,η_1) being replaced by (t_c',η_c') and (t_2,η_2), there are two main differences. Because the cohesion energy of the fluid phase is linear in the density [see Eq. (38)], the Curie line of the fluid phases [see Eq. (48)] is a straight line in the $t-\eta$ plane, whereas the Curie line of the solid phases [see Eq. (52)] has a nonzero curvature, due to the nonlinear density dependence of the lattice energy [see Eq. (39)]. Here the Curie lines of the fluid and solid phases are thus different, whereas in [9] they are identical because the same cohesion energy was used for both the fluid and solid phases (a practice which goes back to Longuet-Higgins and Widom [17]). The most important difference, however,

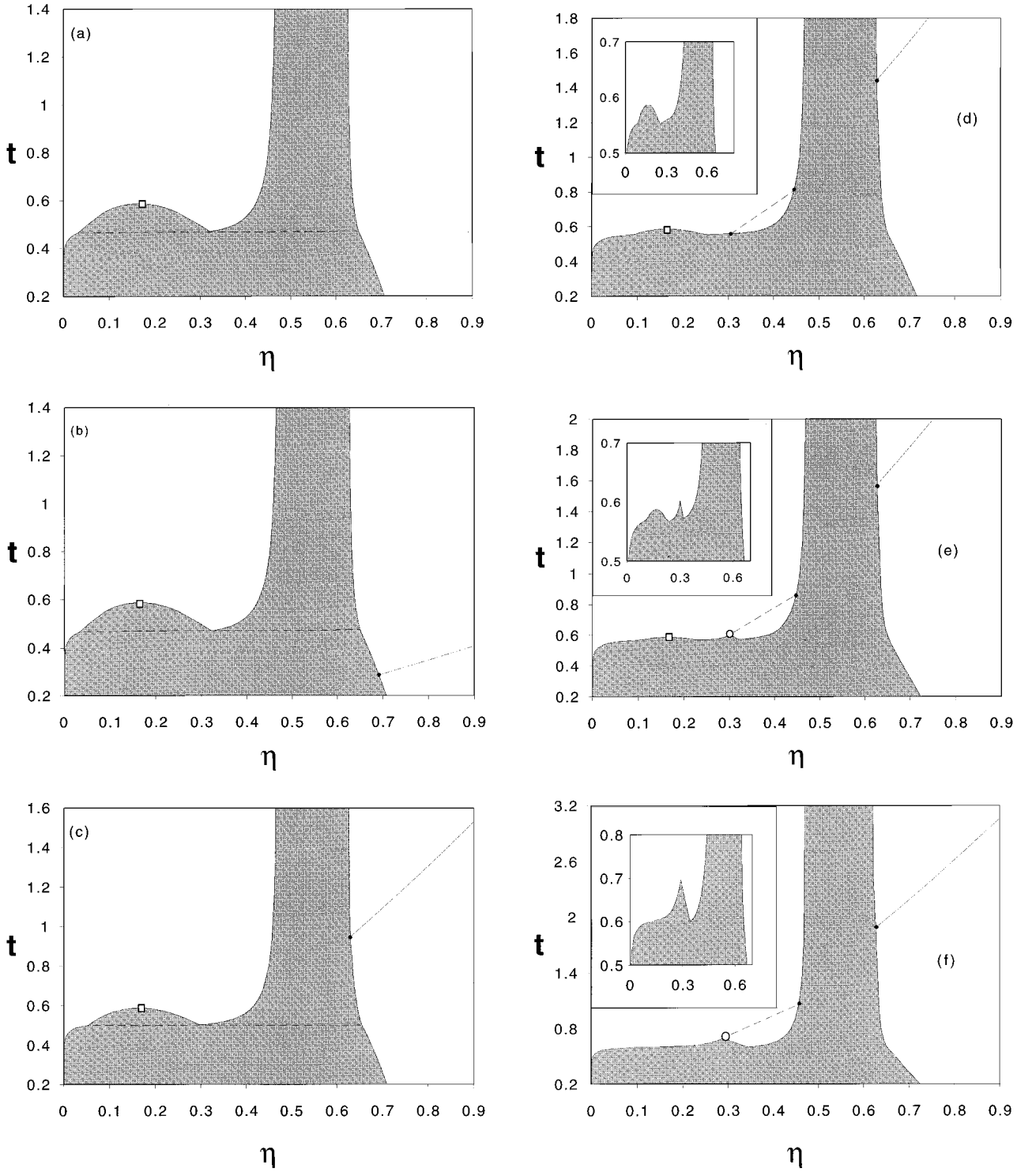

FIG. 4. The topologically distinct types of complete phase diagrams obtained from Eq. (41) by allowing for both fluid and compact solid phases. The case shown corresponds to a situation where both the magnetic ($k=4$) and nonmagnetic ($n=6$) interactions are long ranged. The strengths of the magnetic interaction are (a) $\gamma=0$, (b) $\gamma=0.04$, (c) $\gamma=0.15$, (d) $\gamma=0.23$, (e) $\gamma=0.25$, and (f) $\gamma=0.3$. The meaning of the symbols is the same as in Figs. 2 and 3.

stems from the fact that (for the same reason) the phase diagrams of the solids no longer depend on the parameters $\{\gamma,k,n\}$ through the single combination γ^* of Eq. (49), but they do now depend explicitly on the ranges of the potentials (as set here for the inverse power potentials by their index k and n). Therefore we now have again a phase diagram, with a CP for $0<\gamma<\gamma_1(k,n)$, with both a CP and a TCP for $\gamma_1(k,n)<\gamma<\gamma_2(k,n)$ and with a TCP for $\gamma_2(k,n)<\gamma$, but the threshold values $\{\gamma_1,\gamma_2\}$ now do depend explicitly on k and n. For instance, for $\gamma_1(k,n)$ we find $\gamma_1(4,6)=0.192$,

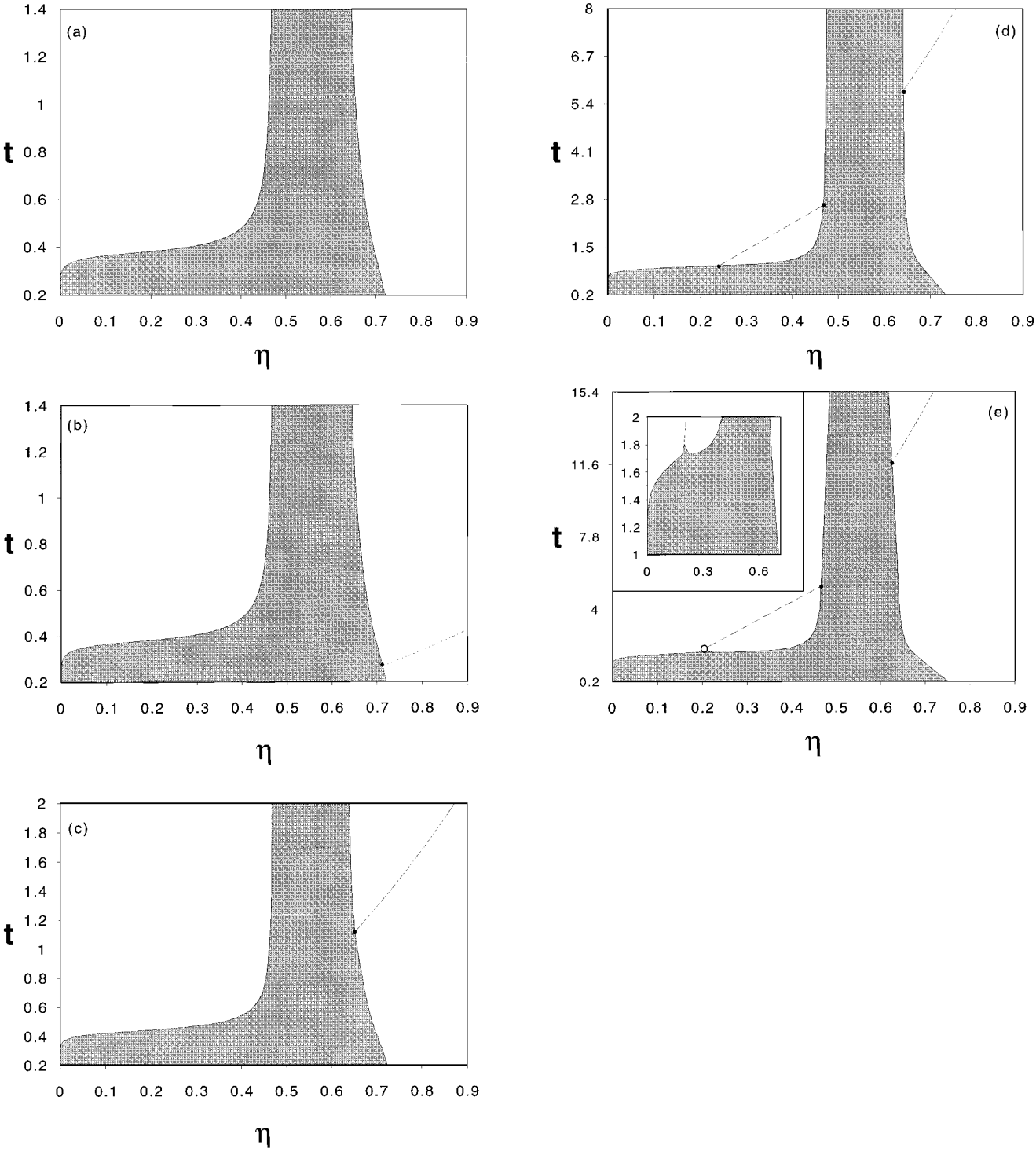

FIG. 5. The same as Fig. 4 but for long-ranged magnetic interactions ($k=6$) and intermediate-ranged nonmagnetic interactions ($n=12$). The strengths of the magnetic interaction are: (a) $\gamma=0$, (b) $\gamma=0.06$, (c) $\gamma=0.3$, (d) $\gamma=1.6$, and (e) $\gamma=3.4$.

$\gamma_1(6,6)=0.325$, $\gamma_1(12,6)=0.365$, whereas for $\gamma_2(k,n)$ we have $\gamma_2(4,6)=0.254$, $\gamma_2(6,6)=0.52$, and $\gamma_2(12,6)=0.955$. An example of the three topologically distinct types of phase diagrams is shown in Fig. 3.

C. Fluid and solid phases

In order to obtain a complete phase diagram we now consider the case where in Eqs. (44) and (45) phase 1 is a fluid phase and phase 2 a solid phase, and combine these fluid-solid transitions with the fluid-fluid and solid-solid transitions already considered in the two previous sections. Stated differently, the fluid-fluid transitions obtained from Eqs. (44) and (45) correspond to double tangent constructions on the free energy (41) when the latter is evaluated for the fluid phase, and similarly for the solid-solid transitions when Eq. (41) is evaluated for the solid phase, whereas the fluid-solid transitions correspond to double tangent constructions be-

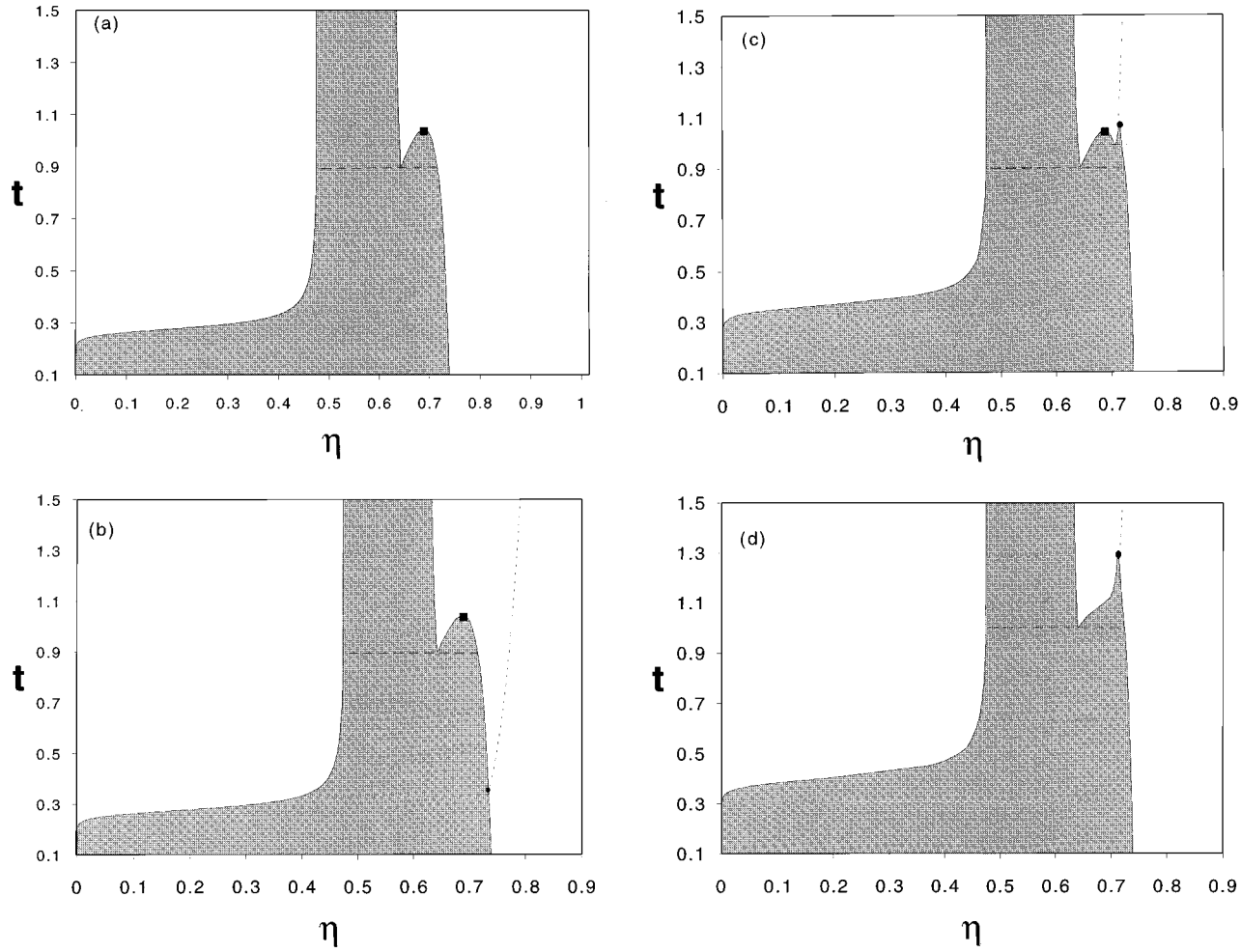

FIG. 6. The same as Fig. 4 but for intermediate-ranged magnetic interactions ($k=60$) and short-ranged nonmagnetic interactions ($n=80$). The strengths of the magnetic interaction are: (a) $\gamma=0$, (b) $\gamma=0.1$, (c) $\gamma=0.55$, and (d) $\gamma=0.7$.

tween the free energy of the fluid and that of the solid. When more than one double tangent construction is possible, the complete phase diagram is obtained from the convex envelope to the free energies. Since the solid-solid transitions do depend on the three parameters $\{\gamma,n,k\}$ separately, so will the complete phase diagrams. We know from [7] that when $\gamma=0$ there are three topologically distinct types of phase diagrams according to the value of n (k is irrelevant when $\gamma=0$). For long-ranged interactions ($3<n<n_1\simeq 7.6$) the phase diagram exhibits the (t_c,η_c) critical point of Eq. (50), for intermediate-ranged interactions ($n_1<n<n_2\simeq 67$) there is no critical point, whereas for short-ranged interactions ($n_2<n$) it exhibits the (t_c',η_c') critical point of (57). We now take a n value corresponding to each category separately (say $n=6$, 12, and 80) and start increasing the value of γ. The sequence of phase diagrams generated in this way depends still on the value of k. Here it will suffice to consider a few specific k values which nevertheless cover all the possible topologically distinct cases. First we consider the long ($n=6$)–long ($k=4$) case where both the value of n and k correspond to long-ranged forces. This case alone generates (see Fig. 4) all the phase diagrams obtained in [9]. Three of them contain a region where the ferromagnetic liquid phase is stable. Next we consider the intermediate ($n=12$)–long ($k=6$) case (see Fig. 5). Here there are two new types of phase diagrams containing a stable ferromagnetic liquid. Finally we consider the short ($n=80$) –intermediate ($k=60$) case (see Fig. 6) where none of the new types of phase diagrams contains a stable ferromagnetic liquid. The latter phase is thus clearly seen to be favored by increasing the range of the nonmagnetic and magnetic interactions.

D. Conclusions

We have considered the phase behavior of a classical system of particles interacting via both (isotropic) nonmagnetic interactions and (anisotropic) magnetic exchange interactions. Such a system constitutes an off-lattice or continuous version of the well-known Heisenberg model of magnetism [1] and, as such, could be considered as a rough approximation to more realistic systems. This Heisenberg fluid is known, for instance, to mimic rather well the behavior of dipolar fluids without having to cope with the difficulties intrinsic to such fluids [10,12]. It is thus a good candidate for studying the influence of the potential parameters on the occurrence of a ferromagnetic liquid in the phase diagram. To obtain these phase diagrams, here we used a simple exten-

sion of the original van der Waals theory [7]. As is well known, in van der Waals theory the free energy is written as the sum of a free-volume entropy term describing the repulsions and a mean-field energy term describing the attractions [2]. What distinguishes the van der Waals theory used here [7] from other approaches [9,17] is the fact that both the free-volume entropy and the mean-field energy have a different density dependence according to whether the phase considered is a fluid or a solid phase. In the presence of the magnetic exchange interactions this difference implies, moreover, that the Curie lines of the fluid and solid phases have a different density dependence. The resulting theory is nevertheless very simple and flexible. It is also fairly realistic since the resulting phase diagrams mimic very closely those obtained from more sophisticated theories, whenever available [6,12]. On this basis we have found that the phase diagrams do depend not only on the relative strength of the magnetic and nonmagnetic interactions but also on the range of these interactions. For instance, it is found that at given relative strength of the magnetic interaction, the ferromagnetic fluid phase is favored by increasing the range of either the magnetic or nonmagnetic interactions. This in turn could well explain why simulations using interactions which are cut off at finite range [12] have difficulties in finding (stable) ferromagnetic fluid phases.

ACKNOWLEDGMENTS

M.B. acknowledges financial support from the Fonds National de la Recherche Scientifique (Belgium).

[1] D. L. Goodstein, *States of Matter* (Dover, New York, 1985); D. A. Young, *Phase Diagrams of the Elements* (University of California Press, Berkeley, 1991).

[2] T. Coussaert and M. Baus, Phys. Rev. E **52**, 862 (1995); M. Baus, T. Coussaert and R. Achrayah, Physica A **232**, 575 (1996).

[3] W. B. Russel, D. A. Saville and W. R. Schowalter, *Colloidal Dispersions*, 2nd ed. (Cambridge University Press, Cambridge, 1991); W. C. K. Poon and P. N. Pusey, in *Observation, Prediction and Simulation of Phase Transition in Complex Fluids*, edited by M. Baus, L. F. Rull, and J. P. Ryckaert (Kluwer, Dordrecht, 1995), p. 3.

[4] J. S. Van Duijneveld, A. W. Heinen, and H. N. W. Lekkerkerker, Europhys. Lett. **21**, 369 (1993); S. M. Ilett, A. Orrock, W. C. K. Poon, and P. N. Pusey, Phys. Rev. E **51**, 1344 (1995).

[5] P. G. Bolhuis, M. H. J. Hagen, and D. Frenkel, Phys. Rev. E **50**, 4880 (1994); C.N. Likos, T. Nemeth, and H. Lowen, J. Phys Condens. Matter **6**, 10 965 (1994).

[6] C. F. Tejero, A. Daanoun, H. N. W. Lekkerkerker, and M. Baus, Phys. Rev. E **51**, 558 (1995); C. Rascon, G. Navascues, and L. Mederos, Phys. Rev. B **51**, 14 799 (1995).

[7] A. Daanoun, C. F. Tejero, and M. Baus, Phys. Rev. E **50**, 2913 (1994); M. Baus and R. Achrayah, J. Phys. Condens. Matter **8**, 9633 (1996); see also [2].

[8] D. Marx, P. Nielaba, and K. Binder, Phys. Rev. **67**, 3124 (1991); R. M. Stratt, Phys. Rev. Lett. **53**, 1305 (1984).

[9] P. C. Hemmer and D. Imbro, Phys. Rev. A **16**, 380 (1977), see also J. S. Hoye and G. Stell, Phys. Rev. Lett. **36**, 1569 (1976); L. Feijoo, C. -W. Woo, and V. T. Rajan, Phys. Rev. B **22**, 2404 (1980).

[10] M. Widom and H. Zhang, Phys. Rev. Lett. **74**, 2616 (1995); B. Groh and S. Dietrich, *ibid*. **74**, 2617 (1995).

[11] D. Wei and G. N. Patey, Phys. Rev. A **46**, 7723 (1992); J. J. Weis and D. Levesque, Phys. Rev. E **48**, 3728 (1993); B. Groh and S. Dietrich, *ibid*. **54**, 1627 (1996).

[12] E. Lomba, J. J. Weis, N. G. Almarza, F. Bresme, and G. Stell, Phys. Rev. E **49**, 5169 (1993); M. J. P. Nijmeijer and J. J.Weis, Phys. Rev. Lett. **75**, 2887 (1995); J. M. Tavares, M. M. Telo da Gama, P. I. C. Teixeira, J. J. Weis, and M. J. P. Nijmeijer, Phys. Rev. E **52**, 1915 (1995).

[13] R. P. Sear, Phys. Rev. Lett. **76**, 2310 (1996): R. van Roij, *ibid.* **76**, 3348 (1996).

[14] S. Chandrasekar, *Liquid Crystals*, 2nd ed. (Cambridge University Press, Cambridge, 1992).

[15] J. A. Cuesta, C. F. Tejero, and M. Baus, Phys. Rev. A **45**, 7395 (1992), and references therein.

[16] H. Zhang and M. Widom, Phys. Rev. E **49**, R3591 (1994).

[17] H. C. Longuet-Higgins and B. Widom, Mol. Phys. **8**, 549 (1964).